Chemical Physics Letters 683 (2017) 579–585

Contents lists available at ScienceDirect

Chemical Physics Letters

journal homepage: www.elsevier.com/locate/cplett

Research paper

Monitoring non-adiabatic dynamics in CS_2 with time- and energy-resolved photoelectron spectra of wavepackets

Kwanghsi Wang [a,*], Vincent McKoy [a], Paul Hockett [b], Albert Stolow [b,c,d], Michael S. Schuurman [b,d]

[a] A.A. Noyes Laboratory of Chemical Physics, California Institute of Technology, Pasadena, CA 91125, USA
[b] National Research Council Canada, 100 Sussex Drive, Ottawa, Ontario K1A 0R6, Canada
[c] Department of Physics, University of Ottawa, ON K1N 6N5, Canada
[d] Department of Chemistry and Biomolecular Sciences, University of Ottawa, Ottawa, ON K1N 6N5, Canada

ARTICLE INFO

Article history:
Received 7 December 2016
In final form 7 February 2017
Available online 9 February 2017

Keywords:
Nonadiabaticity
Conical intersection
Ab initio multiple spawning
Molecular frame photoelectron angular distribution

ABSTRACT

We report results from a novel fully *ab initio* method for simulating the time-resolved photoelectron angular distributions around conical intersections in CS_2. The technique employs wavepacket densities obtained with the multiple spawning method in conjunction with geometry- and energy-dependent photoionization matrix elements. The robust agreement of the calculated molecular-frame photoelectron angular distributions with measured values for CS_2 demonstrates that this approach can successfully illuminate, and disentangle, the underlying coupled nuclear and electronic dynamics around conical intersections in polyatomic molecules.

1. Introduction

Time-resolved photoelectron spectroscopy (TRPES) is a versatile probe of ultrafast dynamics in molecules and has been widely used in recent years to study non-adiabatic dynamics in numerous systems [1–7]. This pump-probe technique first prepares a vibronic wavepacket on an excited-state surface, then ionizes the molecule with a time-delayed probe pulse to determine photoelectron spectra. The photoionization dynamics will clearly evolve as the wavepacket moves through regions of strong non-adiabatic coupling involving conical intersections. Thus, the photoelectron spectra as a function of the time delay are sensitive to both the location of the nuclei and the evolution of the electronic structure, making them well suited for studying wavepacket dynamics around conical intersections where nuclear and electronic degrees of freedom are strongly coupled.

In cases where the coupling of nuclear and electronic degrees of freedom cannot be unambiguously disentangled on the basis of the photoelectron energy analysis alone, photoelectron angular distributions (PADs), particularly in the molecular frame [8,9], can be employed to discern the electronic character of the underlying states. The use of time-resolved PADs in excited state molecular dynamics has been recently reviewed [10–12]. These PADs provide a novel way to follow chemical reaction dynamics in excited states and to monitor the associated non-adiabatic dynamics in the photochemistry. Bisgaard et al. [8] studied time-resolved molecular-frame photoelectron angular distributions (TRMFPADs) to monitor the evolution of the electronic character of the excited states in the non-adiabatic photodissociation reaction of CS_2. The pump-probe photoionizaton dynamics that we study in CS_2 involve pumping to the adiabatic S_2 state that is labeled $C^1\Sigma_u^+$ at linear geometries, where it has $n \rightarrow \pi_u^*$ character; this state has $^1B_2$ symmetry at its bent (C_{2v}) geometries. Higher in energy is S_3 which is $n \rightarrow \pi_g^*$ $^1\Delta_g$ at linear geometries. At bent geometries the $n \rightarrow \pi_u^*$ and $n \rightarrow \pi_g^*$ electronic states couple, and the S_2 and S_3 adiabatic states both become geometry-dependent admixtures of those diabatic states whose character varies strongly in the vicinity of conical intersections. Moreover, the S_3 also interacts with a higher state, S_4, that is $^1\Pi_g$ at linear geometries and so acquires $n \rightarrow \sigma^*$ character upon bending and stretching. The TRMFPADs exhibit strong *d* character at earlier times (~100 fs) and mixed *p* and *d* character at later times (~500 fs), which Bisgaard et al. attributed to this mixing. Their seminal studies illustrated the potential of TRMFPADs for characterizing non-adiabatic dynamics around conical intersections in molecular systems and highlighted the need for numerical simulations of such TRMFPADs. The excited state dynamics of CS_2 were recently studied via time-resolved photoelectron imaging with improved time resolution using sub-20 fs pulses [13].

* Corresponding author.
E-mail addresses: kwang@cookie.caltech.edu (K. Wang), Michael.Schuurman@nrc-cnrc.gc.ca (M.S. Schuurman).

http://dx.doi.org/10.1016/j.cplett.2017.02.014
0009-2614/

Simulations of time-resolved photoelectron spectra in polyatomic molecules that employ a robust description of both the wavepacket dynamics and the photoionization dynamics can be expected to be challenging, particularly around conical intersections where the photoionization dynamics can evolve rapidly with nuclear configuration. In this letter, we employ an *ab initio* approach for simulating time-resolved photoelectron angular distributions involving ionization from multiple electronic states that are coupled by seams of conical intersection. This approach is applicable to diverse systems of photochemical interest. Here, the nuclear dynamics are simulated using the first-principles *ab initio* multiple spawning (AIMS) method [14–18], and wavepacket densities obtained from these simulations at a series of time delays: these are subsequently combined with computed photoionization amplitudes to produce energy-, angle-, and time-resolved photoelectron spectra. We apply this approach to time-resolved molecular frame angular distributions around conical intersections in CS_2. Preliminary results of these studies were reported previously [19].

2. Background and theoretical development

Pump-probe femtosecond time-resolved photoelectron spectroscopy is well suited to probing excited state dynamics in isolated molecules [11,20–24]. In this technique, a femtosecond pump pulse prepares a wavepacket on an excited state which is subsequently probed by ionization with a second, delayed laser pulse. The energy-resolved photoelectron spectra can be used to map the evolution of the vibrational wavepacket and its interaction with other electronic surfaces, particularly through non-adiabatic regions [20,21,25,26]. Sensitivity to both the character of the electronic wave function and vibrational dynamics, combined with the universal nature of photoionization (no dark states), makes pump-probe photoelectron spectroscopy a versatile probe of non-adiabatic processes such as internal conversion and radiationless transitions in molecules [2,11,20,22,23,27]. Moreover, the photoelectron angular distribution provides further information about the character of the electronic states involved and can be a valuable complement to energy-resolved photoelectron spectra in unraveling the underlying dynamics in non-adiabatic regions [11,20,21,25,26]. Our prior work on TRMFPADs showed that this observable, to some degree, 'filters out' the purely electronic dynamics of the valence electrons, even when non-adiabatically coupled to the vibrational dynamics [9].

This study expands upon a formulation of energy- and angle-resolved pump-probe photoelectron spectroscopy which we developed recently [19], employing wavepacket densities obtained with the multiple spawning method in conjunction with geometry- and energy-dependent photoionization matrix elements. This formulation has been successfully used to explore the non-adiabatic dynamics around the conical intersections of the excited states in CS_2 [19]. Below we outline key aspects of this formulation.

2.1. Pump - probe photoelectron spectroscopy

Accurate simulation of time-resolved pump-probe photoelectron spectroscopy requires a good description of both the molecular dynamics initiated by the pump pulse and the ionization dynamics describing the probe process. The first of these ingredients is characterized by vibronic wavepacket densities, while the photoionization dynamics is governed by energy- and geometry-dependent photoionization matrix elements. Combining both ingredients, the energy- and angle-resolved molecular frame photoelectron angular distributions (MFPADs) at a given time t_{pr} can be written as

$$P_{\mathbf{k}}(\theta_k,\phi_k,t_{pr}) = \sum_I \int d\mathbf{R}|\chi_I(\mathbf{R},t_{pr})|^2 \Big|\sum_{\ell m} C_{I,\mathbf{k}\ell m}(\mathbf{R}) Y^*_{\ell m}(\theta_k,\phi_k)\Big|^2, \quad (1)$$

where $|\chi_I(\mathbf{R},t_{pr})|^2$, the only time-dependent quantity, is the wavepacket density at time t_{pr} obtained from the *ab initio* multiple spawning (AIMS) method, to be discussed in Section 2.3, while the coefficients $C_{I,klm}(\mathbf{R})$, to be discussed in Section 2.2, contain information on the photoionization dynamics for the Ith neutral electronic state and depend on molecular geometry and photoelectron energy. In Eq. (1), $\mathbf{k}$ is the momentum of the photoelectron, the angles (θ_k,ϕ_k) define its direction relative to the polarization vector of the probe pulse, $Y_{\ell m}(\theta_k,\phi_k)$ is a spherical harmonic, and $\mathbf{R}$ is the set of internal nuclear coordinates. Eq. (1) carries out a summation over all ionization channels, where the contribution of each channel is determined by the Ith portion of the wavepacket density, $|\chi_I(\mathbf{R},t_{pr})|^2$, on the corresponding neutral potential surface and by the photoionization matrix elements connecting that neutral state to an ionic state. The photoelectron kinetic energy, and thus the magnitude of $\mathbf{k}$, are determined through energy conservation by $\epsilon_k = \frac{1}{2}\hbar k^2/m_e = \hbar\omega_{pr} + V_I(\mathbf{R}) - V_{ion}(\mathbf{R})$, where V_I and V_{ion} are the potential surfaces of the neutral and ionic states, respectively, and $\hbar\omega_{pr}$ is the probe pulse photon energy, which we take to be the central energy (frequency) of the Gaussian probe pulse.

After rotating the frame of the matrix elements to align both the molecular axis (S—S axis) and the polarization of the probe pulse with the laboratory z axis, the laboratory-frame photoelectron angular distributions (LFPADs) for aligned CS_2 are approximated by integrating analytically over ϕ_k angles of the MFPADs, giving

$$P_k(\theta_k,t_{pr}) = \sum_I \int d\mathbf{R}|\chi_I(\mathbf{R},t_{pr})|^2 \sum_{m=-L}^{L}\left|\sum_{\ell=|m|}^{L} C_{I,k\ell m}(\mathbf{R}) Y^*_{\ell m}(\theta_k,0)\right|^2, \quad (2)$$

where L is the maximum partial wave used. Eqs. (1) and (2) interface a rigorous description of molecular photoionization dynamics, contained in the geometry- and energy-dependent matrix elements, with wavepacket densities, $|\chi_I(\mathbf{R},\mathbf{t_{pr}})|^2$, the latter obtained from a first-principles multiple spawning simulation to yield fully *ab initio* determinations of time-, energy- and angle-resolved photoelectron spectra. The generality of this approach suggests that the technique will be widely applicable to molecules of photochemical interest.

2.2. Molecular photoionization amplitudes

A robust description of molecular photoionization amplitudes is essential in non-adiabatic regions, where dramatic changes in the character of the electronic states make the assumption of constant ionization amplitudes problematic [28–31]. Over a number of years, we have developed *ab initio* techniques to obtain these important quantities [32,33] and have successfully applied them to study the time-resolved photoelectron spectroscopy in Na_2 [5,34], NaI [25,26], chloromalonaldehyde [35], NO_2 [36], and CS_2 [19]. For the final state wave functions (ion plus photoelectron), we assume a frozen-core Hartree-Fock model, in which the ion orbitals are taken to be those of the neutral core while the photoelectron orbital is obtained as the solution of a one-electron Schrödinger equation containing the Hartree-Fock potential of the molecular ion. Although such a description may prove adequate for the final state, a configuration interaction wave function must generally be employed to describe the neutral potential surfaces far from equilibrium and in non-adiabatically coupled regions. Our studies have shown that this approach yields a quantitative description of the photoionization amplitudes and their dependence on molecular geometry and photoelectron kinetic energy.

In practice, we do not solve the Schrödinger equation for the photoelectron orbital directly but rather use a procedure [32,33,37] in which the desired photoelectron orbitals are expanded in partial waves and the expansion coefficients obtained from an iterative solution of the Lippmann-Schwinger equation associated with the one-electron Schrödinger equation.

2.3. Ab initio multiple spawning method

The computational complexity of TRPES simulations scales rapidly with the size of the molecule. To make calculations generally applicable to polyatomics, one can employ potential surfaces of reduced dimensionality as a framework into which a description of the photoionization dynamics is embedded. There are several methods for obtaining such surfaces [35,38–40], all of which proceed by identifying a small set of active modes — those which are critical to the dynamics — and treating the others as bath modes. Unfortunately, it can be difficult to constrain the active modes to a manageable number if different modes are pertinent to the dynamics at different times, or if the motion is highly anharmonic. To avoid these difficulties, we employ a computationally efficient full-dimensional treatment of the nuclear dynamics given by the AIMS approach [14–18] to obtain the wavepacket densities at a series of time delays. In principle, AIMS can treat an arbitrary number of nuclear degrees of freedom on multiple electronic states. Most importantly, since the potential energy surface is determined on-the-fly, the need to represent the PES using analytic functional forms is obviated, making it ideal for studies of non-adiabatic dynamics in large polyatomic molecules of photochemical interest such as uracil, thymine, and protein chromophores [41,42].

To situate the AIMS approach within the context of TRPES studies, we briefly outline the method here. For detailed information, see Refs. [43,44]. In AIMS, the total wavefunction is expanded as a sum of Born-Oppenheimer states written as products of adiabatic electronic wavefunctions, ψ_j^I and nuclear basis functions:

$$\Psi(\mathbf{r},\mathbf{R},t)=\sum_{I=1}^{N_s}\sum_{j=1}^{N_I(t)}c_j^I(t)\psi_j^I(\mathbf{r};\mathbf{R}_j^I(t))g_j^I(\mathbf{R};\mathbf{R}_j^I(t),\mathbf{P}_j^I(t),\gamma_j^I(t)). \quad (3)$$

The nuclear basis functions are chosen to be complex multidimensional products of frozen Gaussians [45], g_j^I, that are parameterized by their average positions, $\mathbf{R}_j^I(t)$, momenta, $\mathbf{P}_j^I(t)$, and phase, $\gamma_j^I(t)$, where the I denotes the electronic state on which the Gaussians evolve, and j indexes the basis function.

The average positions and momenta evolve classically according to Hamilton's equations, while the phase factors are propagated semiclassically as the time integral of the Lagrangian. The complex coefficients, $c_j^I(t)$, in the expansion of the total wavefunction are determined variationally from the solution of the time-dependent nuclear Schrödinger equation in the basis of trajectories. Propagation of the nuclear basis functions is performed using energy gradients determined from *ab initio* electronic structure methods at each time step. The magnitude of the non-adiabatic coupling, as computed at the average position of the trajectory basis function, is monitored as the trajectory evolves on a potential energy surface. If this quantity exceeds a defined threshold, indicating a region of strong nonadiabatic coupling, new basis functions are spawned on the electronic state to which it is coupled. Thus, the number of basis functions on electronic state I, $N_I(t)$, will change as a function of the propagation time. Notably, the vibronic wavepacket is defined in Cartesian coordinates, and its propagation requires only local properties of the adiabatic potential surfaces. The generality of the AIMS approach makes it particularly suitable for treatment of polyatomic molecules which, in general, have many conical intersections and a large nuclear configuration space.

To simulate the pump step of a pump-probe experiment, initial positions and momenta of the Gaussian basis functions are sampled from the ground-state Wigner distribution, subject to the constraint that $|\Delta E - h\nu_{pump}| \leqslant \mathrm{FWHM}_{pump}$ (with ΔE the energy difference between the excited and ground states and FWHM_{pump} the estimated bandwidth of the pump pulse), then vertically lifted onto the excited state surface. The simulation thus assumes a pump pulse that is ultrafast in time (and correspondingly broad in energy) but then filters the initial conditions such that the excitation bandwidth at $t = 0$ corresponds to the experimental pump laser bandwidth.

In the present study, the electronic energies, gradients and derivative couplings were obtained from the COLUMBUS electronic structure program [46]. Specifically, the electronic wavefunctions were determined at the first-order MRCI (FO-MRCI) level of theory.

3. Results and discussion

The methods described in the preceding section were applied to simulate time-, energy-, and angle-resolved photoelectron spectra obtained in femtosecond pump-probe photoelectron spectroscopy of CS_2. *Ab initio* photoelectron matrix elements for photoionization out of S_2 and S_3 states of CS_2 were obtained as described in [36].

3.1. Wavepacket dynamics

Fig. 1 shows the calculated wavepacket densities on the adibatic S_2 (red) and S_3 (blue) neutral electronic state surfaces from 10 fs to 140 fs at intervals of 600 a.u. (about 14.5 fs) as a function of one C-S distance, r_1, and S-C-S bending angle, β, with the other C-S distance, r_2, fixed at 3 a.u. These densities were obtained by averaging over 40 initial conditions, sampled from the ground vibrational state on S_0, which resulted in 796 Gaussian trajectory basis functions and were vertically placed on the S_2 surface at $t_{pr} = 0$. These basis functions were propagated on the S_2 potential surfaces and, at times, underwent partial diabatic transfer to the S_3 state near conical intersections, under the control of the AIMS approach.

The non-adiabatic dynamics are shown in Fig. 1. The main motions on S_2 are asymmetric stretching and bending, with symmetric stretching being less important. The bending motion cycles the wavepacket between the Franck-Condon region (near 180 degrees) and smaller angles, while the asymmetric stretching carries the wavepacket to larger bond lengths and, finally dissociation. At 24 fs, the wavepacket has already bifurcated on S_2, and at 35 fs, it begins to nonadiabatically transfer to S_3 at r_1 near 3 a.u. and β near 135°. Note that for smaller bond lengths and linear geometry ($\beta = 180°$), the S_2 and S_3 states have $^1\Sigma_u^+$ and $^1\Delta_g$ symmetry, respectively, so adiabatic mixing of the two states is forbidden. However, upon bending, the upper orbital of the S_3 state acquires mixed σ and π character, leading to the observed conical intersection with S_2. To better illustrate the non-adiabatic dynamics, the high-quality potential energy surfaces for low-lying states of CS_2 used to obtain Fig. 1 are also shown in Fig. 2 [19].

Several other important features are visible in Fig. 1. First, at 39 fs, the S_3 wavepacket non-adiabatically transitions not only for r_1 near 3 a.u., as discussed above, but also near 4.5 a.u., again with a bending angle about 135°. The transition at the larger bond length is not seen at 35 fs because the wavepacket has not yet reached this region. However, photoelectrons associated with S_3 cannot be detected until wavepacket density returns to the Franck-Condon region at 82 fs. Second, at early times the S_2 state bends toward smaller β values, while S_3 moves toward larger angles (i.e., toward linear geometry). Third, the most important

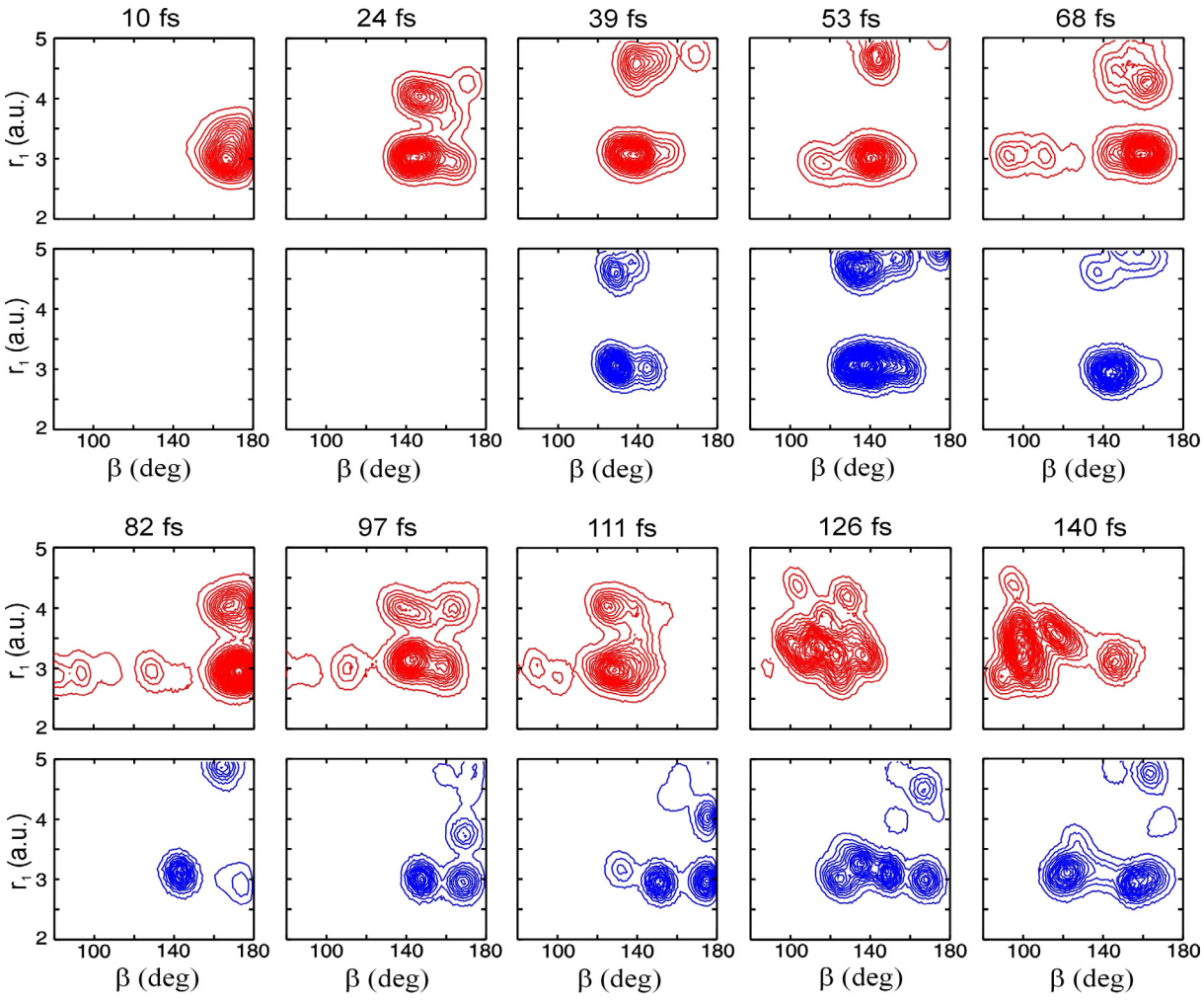

Fig. 1. Wavepacket densities on the S_2 (red) and S_3 (blue) neutral electronic states, respectively, between 10 fs and 140 fs with a constant time interval of 14.5 fs (600 a.u.) as a function of CS distance r_1 and SCS bending angle β with the second CS distance r_2 fixed at 3 a.u. (For interpretation of the references to colour in this figure legend, the reader is referred to the web version of this article.)

dissociation channel is via the lower energy ridge around the linear geometry; it can be seen as wavepacket density disappearing to r_1 values beyond the plotted range with β near 180° on both S_2 and S_3 surfaces. This reflects the linearity of CS_2^+. Fourth, the bending mode is somewhat active during dissociation, implying a breakdown of the axial recoil approximation. Finally, when the S_2 wavepacket propagates to about 130°, it bifurcates into a part with higher kinetic energies that continues toward smaller angles while the other, less energetic part, returns toward larger angles (linear geometry). Once the latter wavepacket arrives back in the Franck-Condon region, ionization by the probe pulse becomes dominant. Similar motions repeat with a period of about 87 fs. This period is relatively long compared to the periods of the stretching motions because the potential surfaces are quite shallow along the bending coordinate. Thus, the MFPADs (see Section 3.2) should readily reflect changes in the electronic composition of the excited states arising from the conical intersections.

3.2. Molecular frame photoelectron angular distributions

Fig. 3 shows calculated molecular frame photoelectron angular distributions at times 0, 106, 145, 213, 314, and 493 fs, with total photoelectron signals shown in black along with the contributions from the S_2 (red) and S_3 (blue) states at photoelectron kinetic energies of 0.05, 0.15, 0.25, and 0.35 eV on the plane where the molecule lies, which corresponds to the $\phi_k = 0$ slice of the entire MFPADs. In each panel, the maximum x or y value is normalized to unity. The vertical direction, $\theta_k = 0°$, is the polarization direction of the probe pulse. Some panels contain only red curves because at that time there is no ionizable wavepacket density on the S_3 state. Besides the initial time $t_{pr} = 0$ and 106 fs, other chosen times are positions of the maximum photoelectron peaks in the vibrational revival patterns in the energy integrated (i.e. ionization yield) photoelectron energy spectra.

These MFPADs are seen to be strongly dependent on the photoelectron kinetic energy. For example, at $t_{pr} = 0$ the angular distribution changes from mainly p-like at 0.05 eV to p with a strong admixture of d character at 0.35 eV. Since the frozen-core approximation was employed in evaluating the photoionization matrix elements, this change reflects not only the ability of the d partial wave to penetrate the angular-momentum barrier at higher photoelectron kinetic energies but also the changing of the electronic composition of the S_2 state at different regions. At times up to 145 fs, ionization from S_2 remains dominant, with d-like character increasing, as indicated by the diagonal lobes. The MFPADs of the S_2 state at 213 and 493 fs are similar, but there the S_3 state makes a comparable contribution to the total. In Refs. [8,9], the authors indicated that the MFPADs of the S_2 state at these later times arise

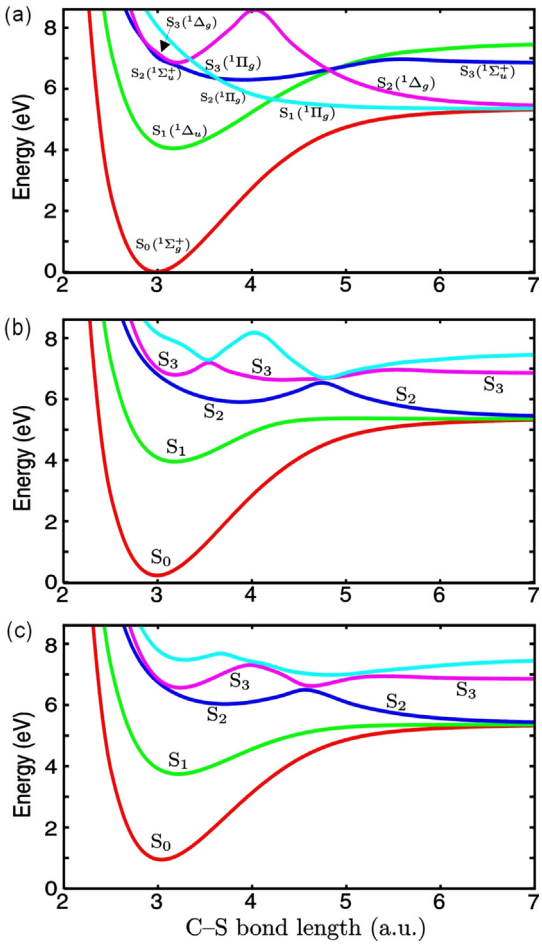

Fig. 2. Potentials for the lowest few $^1A'$ states of neutral CS_2 along the C–S antisymmetric stretch coordinate for bond angles of (a) 180°, (b) 160°, and (c) 140° with the other C–S bond length fixed at 3.0 a.u. Each colored curve represents (a) a diabatic state and (b) and (c) an adiabatic state. (For interpretation of the references to colour in this figure legend, the reader is referred to the web version of this article.)

from ionization of the π^* orbital in the $n \rightarrow \pi^*$ $\left(C^1\Sigma_u^+\right)$ state. On the other hand, the MFPADs from the S_3 state show a mixing of p and d patterns because they reflect ionization from an admixture of σ^* and π^* orbitals arising from non-adiabatic mixing of the $n \rightarrow \pi^*$ state with the $n \rightarrow \sigma^*$ $(^1\Pi_g)$ state at a conical intersection. These distributions are consistent with an atomic picture of ionization, with the p component of the π^* orbital ionizing into a d $(\ell = 2)$ continuum at these times for the S_2 state and of ionization of the s component of σ^* $(^1\Pi_g)$ orbital and the p component of the π^* $(^1\Sigma_u^+)$ orbital into the p and d continua, respectively, for the S_3 state. However, the most striking feature is seen in the PADS of the S_2 state at 314 fs. These MFPADs show much stronger p character and much less d character, differing from the normal pattern of the S_2 PADs. This stronger p character mainly arises from the s component of the S_2 state. The wavepacket density distribution at this time further indicates part of the ionizable wavepackets localizing in the regions which possess $n \rightarrow \sigma^*$ character. It clearly shows that the wavepackets encounter the conical intersection, changing the electronic structure of the S_2 state from purely $n \rightarrow \pi^*$ into an admixture of $n \rightarrow \sigma^*$ and $n \rightarrow \pi^*$. Importantly, these results show clearly how the MFPADs track the non-adiabatic dynamics around a conical intersection in a polyatomic molecule and map the complex evolution of the electronic character of the wavepacket into the photoelectron angular distribution.

Since the MFPADs of the S_2 and S_3 states are quite different, the observed total MFPADs depend on how much each state contributes at any given delay time, which in turn depends on the wavepacket densities on each surface. Even though we do not obtain exact wavepacket densities due to the approximations made in the AIMS method, we can deconvolute the measured angular distributions to analyze the non-adiabatic interaction between the S_2 and S_3 states mediated by the conical intersections.

3.3. Laboratory frame photoelectron angular distributions

Fig. 4 shows the laboratory frame photoelectron angular distributions for aligned CS_2 at delay times 0, 106, 145, 213, 314, and 493 fs, with total photoelectron signals shown in black along with the contributions from the S_2 (red) and S_3 (blue) states at photoelectron kinetic energies of 0.05, 0.15, 0.25, and 0.35 eV. These LFPADs are evaluated analytically from Eq. (2), in which averaging over contributions from all ϕ_k angles has been carried out. Again, the contributions from the S_2 state have predominant d-wave character for most kinetic energies, except for those for 0.05 and 0.15 eV at 493 fs, which show strong p character, while the contributions from the S_3 state show a mixture of p and d waves, ionizing from the s and p partial waves produced by the mixture of the σ^* and π^* orbitals that arises via the conical intersections.

The vertical axis of Fig. 4 coincides with both the molecular axis (S—S) and the polarization of the probe pulse, while the carbon atom lies on the $\pm x$ axis. (Hence, the MFPADs of Fig. 3 are evaluated in the xz plane.) The contributions of the S_3 state to the MFPADs are relatively weak at 106 and 145 fs, while the contributions of that state to the LFPADs are considerable, especially at 106 fs. The explanation is that the S_3 state contributes to the MFPADs much more strongly in the yz plane (i.e., perpendicular to the molecular plane) than in the xz (molecular) plane. However, the situation is reversed for times 314 and 493 fs. Clearly, although not as detailed as the MFPADs, the LFPADs remain a powerful and more experimentally accessible tool for gaining insight into the non-adiabaticity arising from the conical intersections.

3.4. Measured angular distributions

Fig. 5 shows the measured MFPAD with error bars (green bars) and its best fit (green curves) for wavepackets prepared on the $C^1\Sigma_u^+$ state of transiently aligned CS_2 with a 201.2 nm pump pulse and ionized by a probe pulse of 268 nm at a time delay of 100 fs [8,9]. To compare with the measured values, Fig. 5(a) also shows the calculated MFPAD (red) in the molecular plane and the LFPAD (blue), both obtained at a time delay of 106 fs and for a photelectron kinetic energy of 0.15 eV. Both were convoluted with a Gaussian angular function having a standard deviation of 15°, chosen to approximate the lab frame experimental molecular axis distribution and instrument response function. For ease of comparison, Fig. 5(b) shows the original, unconvoluted MFPAD (red) and LFPAD (blue). It clearly seen that the MFPAD in the molecular plane and the LFPAD have quite different shapes; as discussed above, the former is determined primarily by the S_2 state contribution whereas the latter is dominated by the S_3 state.

Interestingly, the MFPADs for the molecular plane seem to agree with the experimental results, although it is not clear why this should be the case, given the experimental geometry. The major discrepancy between the calculated MFPAD and the measured values is along the 90° and 270° directions, where the unconvoluted calculated values show a node that produces a deep minimum in the convoluted results, whereas the measured values show only a small dip. The nodes in the MFPAD and LFPAD are due to the molecular C_s symmetry. However, such a feature may be less

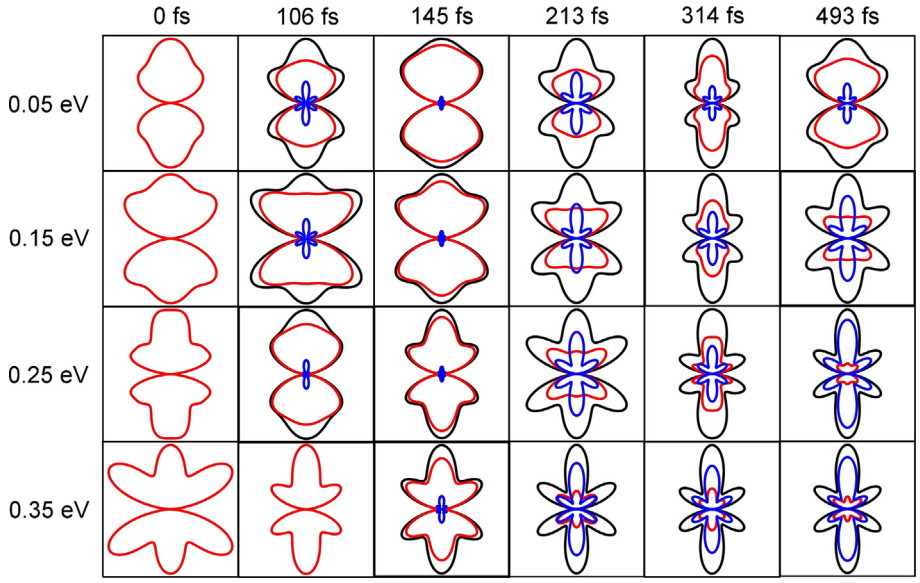

Fig. 3. Molecular frame photoelectron angular distributions at times 0, 106, 145, 213, 314, and 493 fs for total photoelectron signals (black) along with the contributions from the S_2 (red) and S_3 (blue) states at photoelectron kinetic energies of 0.05, 0.15, 0.25, and 0.35 eV. Zero degree is vertical. Some panels contain only red curves because at that time there is no ionizable wavepacket density on the S_3 state surface. (For interpretation of the references to colour in this figure legend, the reader is referred to the web version of this article.)

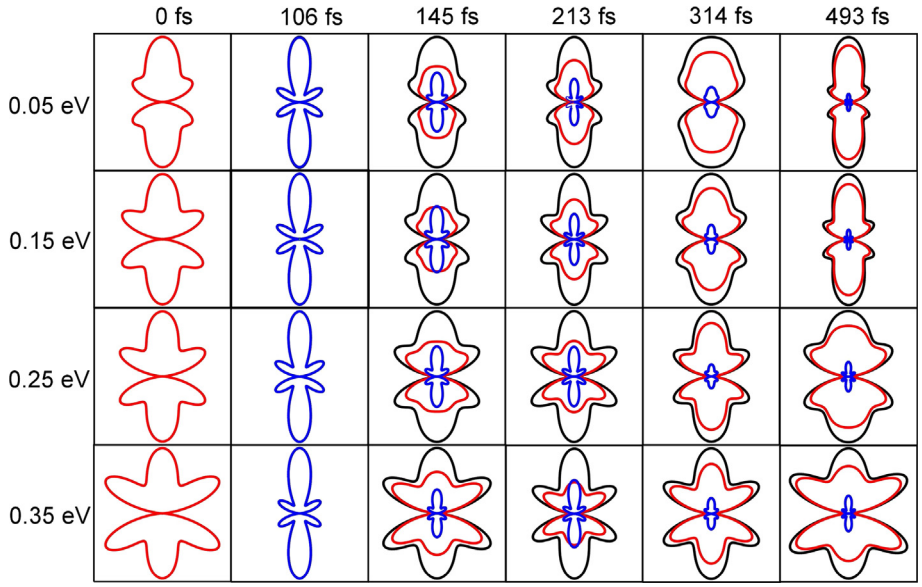

Fig. 4. Laboratory frame photoelectron angular distributions at times 0, 106, 145, 213, 314, and 493 fs for total photoelectron signals (black) along with the contributions from the S_2 (red) and S_3 (blue) states at photoelectron kinetic energies of 0.05, 0.15, 0.25, and 0.35 eV. The vertical, $\theta_k = 0^\circ$, coincides with both the molecular alignment axis and the probe pulse polarization. (For interpretation of the references to colour in this figure legend, the reader is referred to the web version of this article.)

obvious in the measured values due to focal volume averaging of the alignment laser intensity which leads to both radial and axial variation in the contributions of the approximately 20% (on average) unaligned molecules.

Given the experimental setup, in which, following transient alignment, the molecules are free to rotate in any plane containing the alignment axis, it is clear that the measured spectra should be comparable to LFPADs averaged over ϕ_k angles rather than to MFPADs obtained in the molecular plane. We note that the agreement between the measurements and our approximated LFPADs is poorer. This is mainly caused by the approximation used in the wavepacket propagation, in which the wavepacket is instantaneously placed on the S_2 state at $t = 0$ but with an energy width that corresponds to the pump laser bandwidth (i.e., the wavepacket doesn't 'move' during the pump preparation step). The calculated wavepackets thus show higher densities than the actual experimental distribution on the S_3 state at this time. Due to the much stronger distribution of the MFPADs around $\phi_k = 90^\circ$ and 270° than those around $\phi = 0^\circ$, the calculated total LFPADs therefore show a much larger than expected contribution from the S_3 state. Therefore, using the appropriate combination of wavepacket densities from S_2 and S_3 states, the measured spectra can be more accurately simulated. This suggests that, with more accurate preparation of the excited state wavepacket, AIMS calculations of time-, energy-, and angle-resolved photoelectron spectroscopy will lead to important new insights into dynamics at conical intersec-

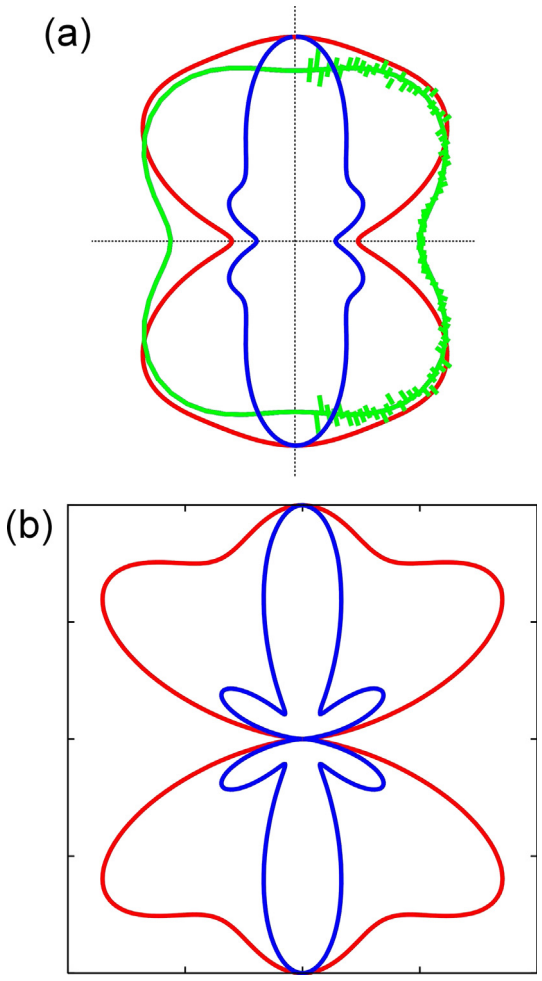

Fig. 5. (a) Measured molecular frame photoelectron angular distribution (green bars) and its best fit (green curves) at a time delay of 100 fs, along with calculated MFPAD (red) and LFPAD (blue) at 106 fs time delay and 0.15 eV photoelectron kinetic energy, both convoluted with a Gaussian function with a standard deviation of 15°. (b) The calculated MFPAD (red) and LFPAD (blue) for a kinetic energy of 0.15 eV at a delay time of 106 fs. (For interpretation of the references to colour in this figure legend, the reader is referred to the web version of this article.)

tions. In general, it is desirable for experimentalists to measure time-resolved MFPADs, as these provide more subtle detail and greater insight into the photochemical dynamics.

4. Conclusion

We have reported the results of simulations of time-resolved molecular frame photoelectron angular distributions for excited state dynamics in CS_2 obtained with an approach that interfaces a rigorous description of photoionization dynamics with wave-packet densities from first-principles multiple spawning calculations. The agreement between the calculated and measured MFPADs is gratifying. These results speak to the value of incorporating energy- and geometry-dependent photoionization matrix elements to obtain more realistic simulations of TRPES spectra. These results also demonstrate the utility of such dynamical simulations in the interpretation and prediction of complex time-resolved spectra. The generality of the computational approach suggests that it will be applicable to a range of molecular systems of photochemical interest.

Acknowledgments

These studies made use of the resources of the Jet Propulsion Laboratory's Supercomputing and Visualization Facility. AS and MS thank the NSERC Discovery Grants program for financial support.

References

[1] A. Assion, M. Geisler, J. Helbing, V. Seyfried, T. Baumert, Phys. Rev. A 54 (1996) R4605.
[2] V. Blanchet, M.Z. Zgierski, T. Seideman, A. Stolow, Nature (London) 401 (1999) 52.
[3] J.A. Davies, J.E. LeClaire, R.E. Continetti, C.C. Hayden, J. Chem. Phys. 111 (1999) 1.
[4] T. Suzuki, L. Wang, K. Kohguchi, J. Chem. Phys. 111 (1999) 4859.
[5] Y. Arasaki, K. Takatsuka, K. Wang, V. McKoy, J. Chem. Phys. 112 (2000) 8871.
[6] S. Lochbrunner, T. Schultz, M. Schmitt, J.P. Shaffer, M.Z. Zgierski, A. Stolow, J. Chem. Phys. 114 (2001) 2519.
[7] M.S. Schuurman, A. Stolow, Conical Intersections: Theory, Computation and Experiment, in: W. Domcke, D. Yarkony, H. Köppel (Eds.), World Scientific, Singapore, 2011, pp. 633–667 (Chapter 16).
[8] C.Z. Bisgaard, O.J. Clarkin, G. Wu, A.M.D. Lee, O. Geßner, C.C. Hayden, A. Stolow, Science 323 (2009) 1464.
[9] P. Hockett, C.Z. Bisgaard, O.J. Clarkin, A. Stolow, Nat. Phys. 7 (2011) 2011.
[10] T. Seideman, Annu. Rev. Phys. Chem. 53 (2002) 41.
[11] A. Stolow, J.G. Underwood, Advances in Chemical Physics, 139, John Wiley & Sons, New York, 2008 (497).
[12] K.L. Katharine, Mol. Phys. 110 (2012) 131.
[13] R. Spesyvtsev, T. Horio, Y.I. Suzuki, T. Suzuki, J. Chem. Phys. 142 (2015) 074308.
[14] T.J. Martínez, M. Ben-Nun, R.D. Levine, J. Phys. Chem. 100 (1997) 7884.
[15] T.J. Martínez, M. Ben-Nun, R.D. Levine, J. Phys. Chem. A 101 (1997) 6389.
[16] M. Ben-Nun, T.J. Martínez, J. Chem. Phys. 108 (1998) 7244.
[17] M. Ben-Nun, T.J. Martínez, J. Chem. Phys. 110 (1999) 4134.
[18] M. Ben-Nun, J. Quenneville, T.J. Martínez, J. Phys. Chem. A 104 (2000) 5161.
[19] K. Wang, V. mcKoy, P. Hockett, M.S. Schuurman, Phys. Rev. Lett. 112 (2014) 113007.
[20] A. Stolow, Annu. Rev. Phys. Chem. 54 (2003) 89.
[21] T. Seideman, Annu. Rev. Phys. Chem. 53 (2002) 41.
[22] D.M. Neumark, Annu. Rev. Phys. Chem. 52 (2001) 255.
[23] M. Wollenhaupt, V. Engel, T. Baumert, Annu. Rev. Phys. Chem. 56 (2005) 25.
[24] I.V. Hertel, W. Radloff, Rep. Prog. Phys. 69 (2006) 1897.
[25] Y. Arasaki, K. Takatsuka, K. Wang, V. McKoy, Phys. Rev. Lett. 90 (2003) 248303.
[26] Y. Arasaki, K. Takatsuka, K. Wang, V. McKoy, J. Chem. Phys. 119 (2003) 7913.
[27] A.M.V. Lee, J.D. Coe, S. Ullrich, M.-L. Ho, S.-J. Lee, B.-M. Cheng, M.Z. Zgierski, I.-C. Chen, T.J. Martínez, A. Stolow, J. Phys. Chem. A 111 (2007) 11948.
[28] P. Cong, G. Roberts, J.L. Herek, A. Mohktari, A.H. Zewail, J. Phys. Chem. 100 (1996) 7832.
[29] V. Blanchet, M.Z. Zgierski, A. Stolow, J. Chem. Phys. 114 (2001) 1194.
[30] L. Pesce, Z. Amitay, R. Uberna, S.R. Leone, J. Chem. Phys. 114 (2001) 1259.
[31] M. Wollenhaupt, A. Assion, O. Graefe, D. Liese, C. Sarpe-Tudoran, M. Winter, T. Baumert, Chem. Phys. Lett. 376 (2003) 457.
[32] R.R. Lucchese, G. Raseev, V. McKoy, Phys. Rev. A 25 (1982) 2572.
[33] K. Wang, V. McKoy, Annu. Rev. Phys. Chem. 46 (1995) 275.
[34] Y. Arasaki, K. Takatsuka, K. Wang, V. McKoy, Chem. Phys. Lett. 302 (1999) 363.
[35] M.T. do, N. Varella, Y. Arasaki, H. Ushiyama, K. Takatsuka, K. Wang, V. McKoy, J. Chem. Phys. 126 (2007) 054303.
[36] Y. Arasaki, K. Takatsuka, K. Wang, V. McKoy, J. Chem. Phys. 132 (2010) 124307.
[37] R.R. Lucchese, D.K. Watson, V. McKoy, Phys. Rev. 22 (1980) 421.
[38] B.A. Ruf, W.H. Miller, J. Chem. Soc., Faraday Trans. 84 (1988) 1523.
[39] G.K. Paramonov, H. Naundorf, O. Kühn, Eur. Phys. J. D 14 (2001) 205.
[40] H. Naundorf, G.A. Worth, H.-D. Meyer, O. Kühn, J. Phys. Chem. A 106 (2002) 719.
[41] H.R. Hudock et al., J. Phys. Chem. 111 (2007) 8500'.
[42] C. Ko, A.M. Virshup, T.J. Martínez, Chem. Phys. Lett. 460 (2008) 272.
[43] M. Ben-nun, T.J. Martínez, Advances in Chemical Physics, 121, John Wiley & Sons, New York, 2002 (439).
[44] B.G. Levine, J.D. Coe, A.M. Virshup, T. Martínez, Chem. Phys. 347 (2008) 3.
[45] E.J. Heller, J. Chem. Phys. 75 (1981) 2923.
[46] H. Lischka, R. Shepard, I. Shavitt, R.M. Pitzer, M. Dallos, Th. Müller, P.G. Szalay, F.B. Brown, R. Ahlrichs, H.J. Böhm, A. Chang, D.C. Comeau, R. Gdanitz, H. Daschel, C. Ehrhardt, M. Ernzerhof, P. Höchtl, S. Irle, G. Kedziora, T. Kovar, V. Parasuk, M.J.M. Pepper, P. Scharf, H. Schiffer, M. Schindler, M. Schüler, M. Seth, E.A. Stahlberg, J.-G. Zhao, S. Yabushita, Z. Zhang, M. Barbatti, S. Matsika, M.S. Schuurman, D.R. Yarkony, S.R. Brozell, E.V. Beck, J.-P. Blaudeau, M. Ruckenbauer, B. Sellner, F. Plasser, J.J. Szymczak, COLUMBUS, An Ab Initio Electronic Structure Program, Release 7.0, 2012.